Electronic Supplementary Material (ESI) for New Journal of Chemistry


# Electronic Supporting Information

## Monodisperse Transfer of Superparamagnetic Nanoparticles from Non-polar Solvent to Aqueous Phase

Erwin Peng, Eugene Shi Guang Choo, Yang Sheng, and Jun Min Xue*

*Department of Materials Science and Engineering, Faculty of Engineering, National University of Singapore (NUS), 7 Engineering Drive 1, Singapore 117574.*

* Email: msexuejm@nus.edu.sg

## S1. Literature Review – Water Solubilization of Hydrophobic Nanocrystals Using Amphiphilic Polymers

**Table S1.** Some of the previously reported phase transfer protocols using amphiphilic polymers and its reported hydrodynamic diameter size in various aqueous solvents.

| Nano crystals | Coatings[a] | Solvent | Average $d_{hyd}$ (nm)[b] | Size Change w.r.t Hydrophobic Nanocrystals [c] | Ref |
|---|---|---|---|---|---|
| **Au** | Oleic Acid | $CHCl_3$ | 7.6 ± 1.8 | - | |
| | PMAT ($C_{14}$) | Borate Buffer | 13.6 ± 1.6 | 78.95% | [1] |
| | PMAO ($C_{18}$) | Borate Buffer | 15.8 ± 2.2 | 107.89% | |
| **ϒ-$Fe_2O_3$** | Oleic Acid | $CHCl_3$ | 9.2 ± 0.6 | - | |
| | PMAT ($C_{14}$) | Borate Buffer | 17.9 ± 0.3 | 94.57% | [1] |
| | PMAO ($C_{18}$) | Borate Buffer | 19.7 ± 0.3 | 114.13% | |
| **ϒ-$Fe_2O_3$** | Oleic Acid | $CHCl_3$ | 12.9 ± 0.8 | - | |
| | PMAT ($C_{14}$) | Borate Buffer | 22.5 ± 0.1 | 74.42% | [1] |
| | PMAO ($C_{18}$) | Borate Buffer | 28.7 ± 1.9 | 122.48% | |
| **CdSe/ZnS QDs** | Organic Coatings | - | ~7nm (TEM) | - | |
| | PSMA/Ethanolamine (mw 1700) | PBS 1x | 13.4 ± 3.4 | ~82.67% | [2] |
| | PSMA/Polyetheramine M-1000 | PBS 1x | 17.8 ± 4.3 | ~137.33% | |
| | PMAO/Ethanolamine | PBS 1x | 24.5 ± 8.2 | ~250.00% | |
| **Green CdSe/ZnS** | TOPO | $CHCl_3$ | 5.7 ± 0.5 | - | |
| | PMAT ($C_{14}$) | Water | 19.2 ± 2.0 | 236.84% | [3] |
| **Red CdSe/ZnS** | TOPO | $CHCl_3$ | 11.6 ± 2.8 | - | |
| | PMAT ($C_{14}$) | Water | 23.6± 2.0 | 103.45% | |
| **$Fe_3O_4$** | Oleic Acid | $CHCl_3$ | ~8nm (TEM) | - | |

| | | | | | |
|---|---|---|---|---|---|
| | PMAO ($C_{18}$) | Water | 43.7 | 446.25% | [4] |
| | | PBS 1x | 42.1 | 426.25% | |
| **Red CdSe/CdS or CdSe/ZnS QDs** | TOPO | $CHCl_3$ | 5.8 (head width to **8.4** (long axis) | - | [5] |
| | PMAO-g-PEG (PEG mw 700) | Water | 24.0 | 185.71% | |
| | PMAO-g-PEG (PEG mw 2000) | Water | 28.5 | 239.29% | |
| | PMAO-g-PEG (PEG mw 6000) | Water | 38.7 | 360.71% | |
| | PMAO-g-PEG (PEG mw 9900) | Water | 42.1 | 401.19% | |
| | PMAO-g-PEG (PEG mw 19300) | Water | 45.9 | 446.43% | |
| **$Fe_3O_4$** | Oleic Acid | $CHCl_3$ | ~21.6 (TEM) | - | [6] |
| | PMAO ($C_{18}$) | Water | 34.0 | 57.41% | |
| | PMAO-g-PEG | Water | 39.8 – 69.3 (Depending on the amount of grafting) | 84.26% - 220.83% | |
| **$Fe_3O_4$** | Oleic Acid | - | ~10 (TEM) | - | [7] |
| | Oleic Acid | - | ~13 (DLS) | - | |
| | F127 | Water | ~36 (DLS) | ~276.92% | |

[a] TOPO: trioctylphosphine oxide; PMAT: poly (maleic anhydride-*alt*-1-tetradecene); PSMA: poly (styrene-*co*-maleic anhydride) or poly (styrene-*alt*-maleic anhydride); PMAO: poly (maleic anhydride-*alt*-1-octadecene); PEG: polyethylene glycol.

[b] As reported by DLS for water soluble nanocrystals or as reported by TEM for hydrophobic nanocrystals.

[c] Calculated against the hydrophobic nanocrystals average size obtained from TEM or DLS experiment.

There were many other reported phase transfer of hydrophobic nanocrystals using amphiphilic polymers into aqueous phase (e.g water, PBS 1x solution or other type of buffer solutions) which did not disclose the hydrodynamic diameter size of the nanocrystals (either in non-polar organic solvent such as hexane and chloroform or in aqueous phase such as water) [8]. Therefore, such results are not included in the previous **Table S1**.

**S2. Calculation on the Total Amount of Hydrolyzing Agent Needed**

The calculation below serves as a guideline in determining the total amount of the hydrolyzing agent needed during water solubilization. Based on our experiments, such calculation can be extended to other type of polymers, e.g. poly (maleic anhydride-*alt*-1-octadecene) as shown in section **S8** in this supporting information.

- *1 mmol of PIMA = 39 mmol equivalent of maleic anhydride (n = 39)*
- *1 mmol of maleic anhydride = 2 mmol equivalent carboxylic acid (after hydrolysis)*
- *1 mmol maleic anhydride reaction with DDA would result in 1 mmol carboxylic acid*
- *75% DDA ($C_{12}$) grafting of PIMA would leave 25% of the remaining maleic anhydride unreacted.*
- *Total amount of carboxylic acid in PIMA-g-$C_{12}$ (75%) after hydrolysis is equal to carboxylic acid from the maleic anhydride ring opening due to reaction with DDA ($C_{12}$)an due to hydrolysis =* $\frac{3}{4}.39 + 2.\frac{1}{4}.39 = \frac{5}{4}.39$ *= 48.75 mmol.*
- *Minimum amount of sodium hydroxide needed is approximately equal to the total amount of carboxylic acid in PIMA-g-$C_{12}$ after hydrolysis = 48.75 mmol.*

## S3. Illustration of Magnetic Nanocrystals Encapsulation by PIMA-g-$C_{12}$

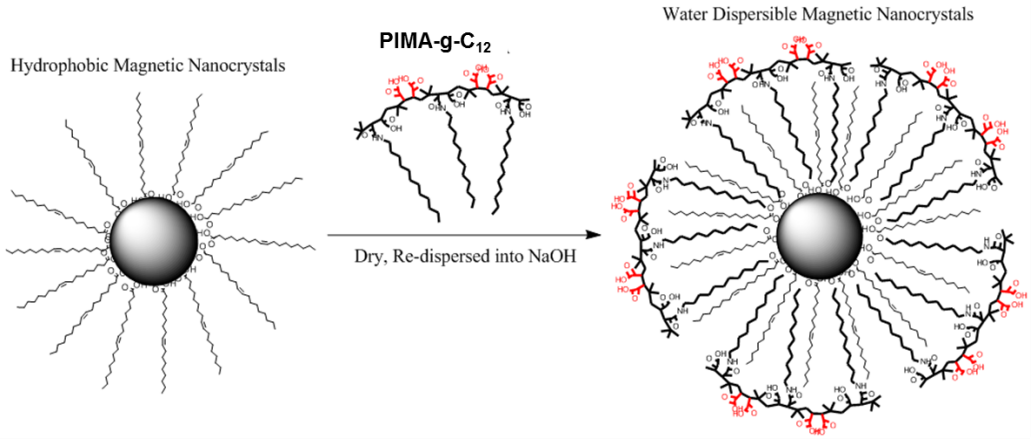


**Fig. S1** Schematic diagram of how PIMA-g-C12 stabilizes hydrophobic magnetic nanocrystals in aqueous solution.

As shown in **Fig. S1**, amphiphilic brush co-polymers PIMA-g-$C_{12}$ could encapsulate hydrophobic nanocrystals through the hydrophobic-hydrophobic interaction formed by the hydrophobic surfactant on nanocrystals surface and the hydrophobic alkane chain ($C_{12}$) from the PIMA-g-$C_{12}$. Meanwhile the presence of maleic anhydride functional group that could be hydrolyzed into carboxylic acids would eventually stabilize the hydrophobic nanocrystals in the aqueous media.

## S4. Further Characterization of IONPs

The as-synthesized oleic-acid coated hydrophobic iron oxide nanocrystals (IONPs) from the high temperature thermal decomposition of iron carboxylate salts was found to have an average size of 10.2 ± 0.8 nm. The TEM size distribution of IONPs was obtained by analyzing 150-200 IONPs nanocrystals from low magnification TEM images (not included) and the size distribution plot was given in **Fig. S2a**. The magnetic property of IONPs was measured by VSM experiment at 300K and the resultant hysteresis loop profile was given in **Fig. S2b**. IONPs exhibited superparamagnetism with no coercivity and zero remnant magnetization ($M_R$). The saturation magnetization ($M_S$) was found to be 42.15 emu.g$^{-1}$.

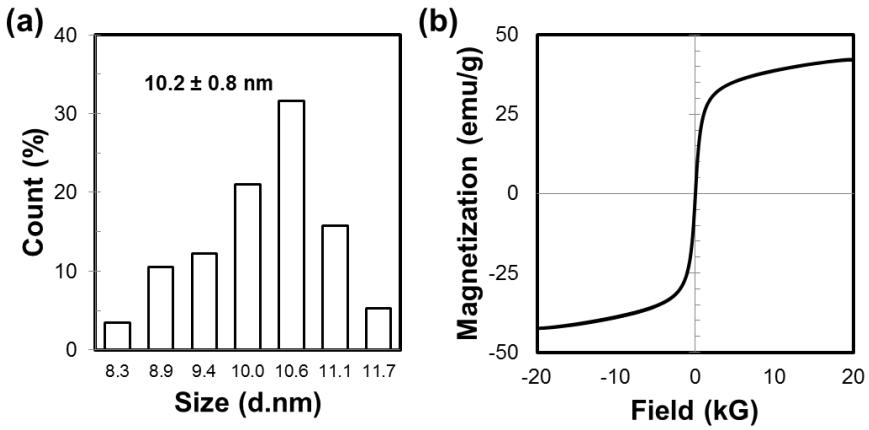


**Fig. S2** (a) TEM size distribution of hydrophobic IONPs in chloroform. (b) Hysteresis loop profile of IONPs recorded at 300K from VSM experiment.

## S5. PIMA-g-$C_{12}$ $^1$H-NMR Spectra Analysis

On top of FT-IR spectra analysis, the chemical structure of PIMA-g-$C_{12}$ was further analyzed by $^1$H-NMR (Bruker DPX300 NMR spectrometer; 300MHz). The chemical shift was analyzed by referencing to the solvent peak (δ = 7.24 ppm for Chloroform-d).

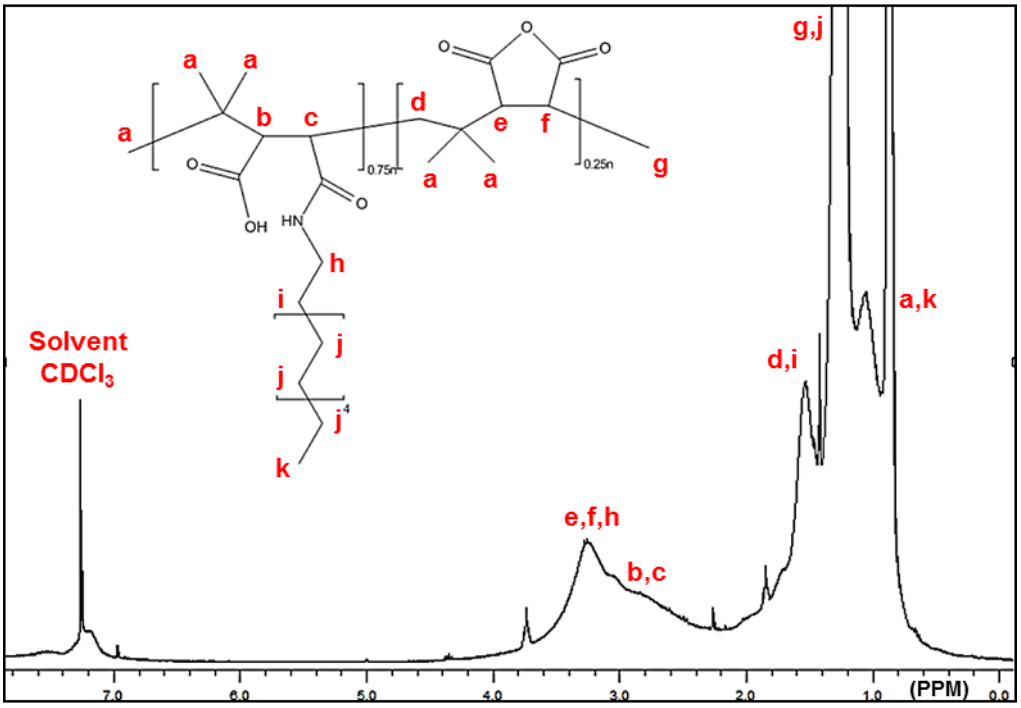


**Fig. S3** $^1$H-NMR spectra of PIMA-g-$C_{12}$ (solvent: chloroform-d, 300MHz).

From the NMR spectrum (**Fig. S3**), the characteristic peaks due to the resonance of alkyl chain ($C_{12}$) of the hydrophobic section of PIMA-g-$C_{12}$ were observed around 0.84 ppm to 1.64 ppm. Moreover, the characteristic peaks of PIMA were successfully identified (see below). The peak of amide bond following the anhydride ring-opening reaction with 1-dodecylamine was not observed due to the lack of such amide bond abundance as compared to the proton of the alkyl chain $C_{12}$ and the PIMA backbone.

$^1$H-NMR (300MHz, $CDCl_3$, δ): 0.84 ppm (–$(CH)_{11}$–C$\underline{H}_3$)), 0.9 - 1.1 ppm (–$CH_2$–C(C$\underline{H}_3$)$_2$), 1.22 ppm (–C$\underline{H}$2–C$\underline{H}_2$–), 1.41 – 1.64 ppm (–C$\underline{H}_2$–C$(CH_3)_2$, –HN–$CH_2$–C$\underline{H}_2$–$CH_2$–), 2.55 - 2.74 ppm (HOOC–C$\underline{H}$–C$\underline{H}$–), 2.97 – 3.17 ppm (–C$\underline{H}$–C$\underline{H}$–$CH_3$, –HN–C$\underline{H}_2$–$CH_2$–$CH_2$–), 7.24 ppm (solvent peak).

## S6. Optimization of the WIONPs Hydrodynamic Size

In this section, various parameters to optimize WIONPs hydrodynamic size would be described. In general, there are three important parameters to be fine-tuned during the water solubilization process: (i) Amount of hydrolyzing agent (sodium hydroxide; NaOH) used during the dissolution of PIMA-g-$C_{12}$/MNPs film; (ii) Amount of PIMA-g-$C_{12}$ with respect to MNPs (mass ratio); and lastly (iii) initial MNPs concentration used to start water solubilization process.

(a)

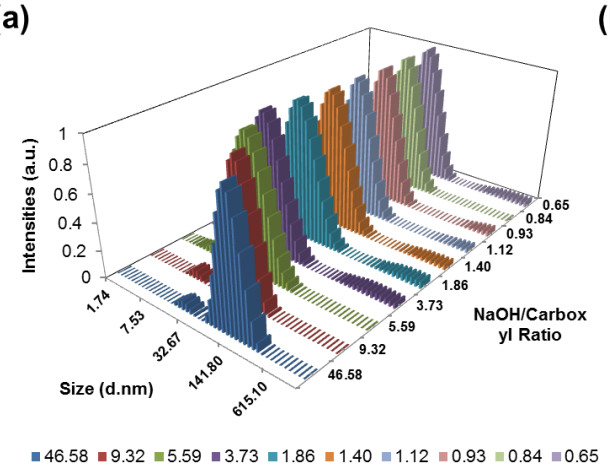


(b)

| NaOH/ Carboyxl Molar Ratio | Average $d_{hyd}$ (d.nm) |
|---|---|
| 0.65 | 27.2 ± 0.2 nm |
| 0.84 | 25.8 ± 0.3 nm |
| 0.93 | 25.6 ± 0.2 nm |
| 1.1 | 23.6 ± 0.1 nm |
| 1.40 | 21.0 ± 0.1 nm |
| 1.86 | 18.5 ± 0.1 nm |
| 3.73 | 20.1 ± 0.2 nm |
| 5.59 | 23.0 ± 0.4 nm |
| 9.32 | 48.6 ± 1.0 nm |
| 48.58 | 114.6 ± 1.3 nm |

**Fig. S4** (a) Size distribution of WIONPs at different NaOH/carboxyl molar ratio. (b) Tabulated average hydrodynamic size of WIONPs against the NaOH/carboxyl molar ratio.

Firstly, we assessed the importance of the hydrolyzing agent amount towards the hydrodynamic size of the resultant WIONPs. **Fig. S4a** showed the size distribution variation of the resultant water soluble WIONPs as the amount of hydrolyzing agent sodium hydroxide was changed (while maintaining equal total volume of the system). The resultant WIONPs hydrodynamic sizes were tabulated against the NaOH/carboxyl molar ratio as shown in **Fig. S4b**. It was revealed that there was an optimum sodium hydroxide/carboxyl molar ratio (approximately ~2) in order to minimize the overall WIONPs hydrodynamic size. The results presented in **Fig. S4** clearly explained the effect of sodium hydroxide amounts. However the experiments

were carried out while maintaining equal total volume of the system, which implies variation of overall sodium hydroxide concentration for each data set. It is not clear whether there is any concentration effect towards the overall hydrodynamic size.

(a)

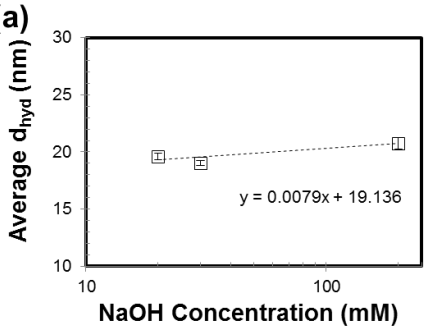


(b)

| NaOH Concentration (mM) | Average $d_{hyd}$ (d.nm) |
|---|---|
| 20.0 mM | 19.6 ± 0.3 nm |
| 33.3 mM | 19.1 ± 0.2 nm |
| 200.0 mM | 20.7 ± 0.5 nm |
| **Total NaOH Used – 0.2 mmol** | |

**Fig. S5** (a) Average hydrodynamic size of WIONPs at different NaOH/carboxyl molar ratio. (b) Tabulated average hydrodynamic size of WMFNPs against the NaOH/carboxyl molar ratio.

In a further experiment, such optimum sodium hydroxide/carboxyl molar ratio was found to be independent of the concentration of the hydrolyzing agent. Overall, our results suggested that the concentration of the hydrolyzing agent sodium hydroxide is less significant than total amount of sodium hydroxide/carboxylic acid molar ratio (data is not shown). As demonstrated in **Fig. S5**, the hydrolyzing agent sodium hydroxide concentration has minimum effect towards the overall hydrodynamic size of WIONPs, when the concentration of sodium hydroxide used was varied while maintaining total amount of sodium hydroxide used (0.2 mmol).

(a)

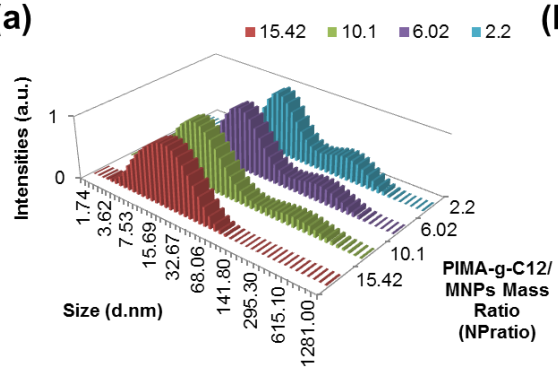


(b)

| PIMA-g-$C_{12}$/ MNPs Mass Ratio ($NP_{ratio}$) | Average $d_{hyd}$ (d.nm) |
|---|---|
| 2.2 | 33.0 ± 0.6 nm |
| 6.0 | 21.7 ± 0.1 nm |
| 10.1 | 16.2 ± 0.2 nm |
| 15.4 | 14.7 ± 0.2 nm |

**Fig. S6** (a) Size distribution of WIONPs at different PIMA-g-$C_{12}$/MNPs mass ratio

($NP_{ratio}$). (b) Tabulated average hydrodynamic size of WIONPs against the $NP_{ratio}$.

Apart from the sodium hydroxide/carboxyl molar ratio, we also investigated the effect of PIMA-g-$C_{12}$/MNPs mass ratio (**$NP_{ratio}$**) towards the encapsulation efficiency. The results presented in **Fig. S4** ($NP_{ratio}$ = 5) were repeated with $NP_{ratio}$ of 10 and the similar trend predicted in **Fig. 3a** for the optimum sodium hydroxide/carboxyl molar ratio were obtained (data is not shown). Based on the optimum sodium hydroxide/carboxyl molar ratio of 2, the water solubilization experiment was repeated by varying the $NP_{ratio}$ and the overall hydrodynamic size were plotted in in **Fig. S6a**. As the $NP_{ratio}$ increased, the average hydrodynamic size of WIONPs decreased rapidly suggesting that more amphiphilic brush co-polymers PIMA-g-$C_{12}$ would be needed in order to suppress the hydrodynamic size of the nanocrystals after water solubilization.

(a)

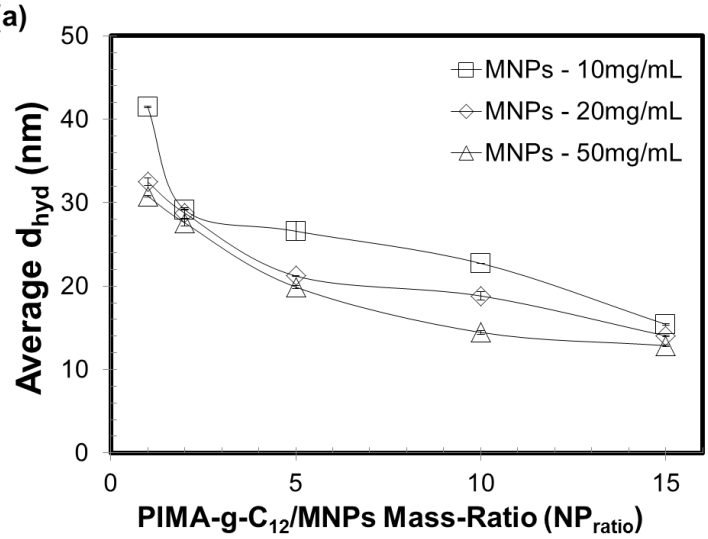


(b)

| $NP_{ratio}$ | Initial MNPs Concentration | | |
|---|---|---|---|
| | 10mg/mL | 20mg/mL | 50mg/mL |
| 1 | 41.5 ± 0.1nm | 32.5 ± 0.5 nm | 30.8 ± 0.1 nm |
| 2 | 29.2 ± 0.1nm | 28.8 ± 0.7 nm | 27.6 ± 0.4 nm |
| 5 | 26.6 ± 1.1nm | 21.2 ± 0.1 nm | 19.9 ± 0.2 nm |
| 10 | 22.7 ± 0.0nm | 18.8 ± 0.5 nm | 14.5 ± 0.2 nm |
| 15 | 15.4 ± 0.1nm | 14.0 ± 0.1 nm | 12.9 ± 0.1 nm |

**Fig. S7** (a) Size distribution of WIONPs against PIMA-g-$C_{12}$/MNPs mass ratio ($NP_{ratio}$) at different initial MNPs concentration (i.e. 10, 20 and 50 $mg.mL^{-1}$). (b) Tabulated average hydrodynamic size of WIONPs against the $NP_{ratio}$ and the initial

MNPs concentration.

Lastly, in order to evaluate the effect of the initial MNPs towards the overall water solubilization efficiency, three different initial MNPs concentrations were employed (10, 20 and 50 mg/mL$^{-1}$). The water solubilization of IONPs was then conducted with various initial MNPs concentration and adjusted $NP_{ratio}$ (sodium hydroxide/carboxyl molar ratio was fixed at ~2). Similar to previous case, as $NP_{ratio}$ increases, the hydrodynamic size of WIONPs would decrease and in the end it would converge into s single hydrodynamic size. In general, as the initial MNPs concentration was increased, the overall $NP_{ratio}$-dependent hydrodynamic size profile would shift down towards smaller hydrodynamic sizes.

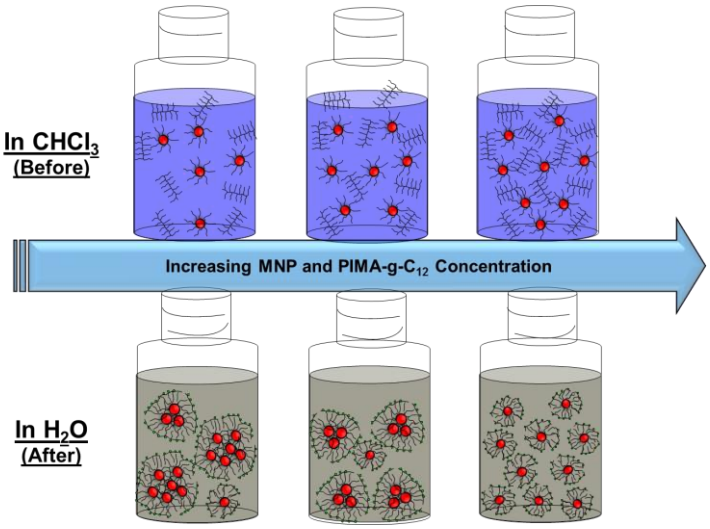


**Fig. S8** Schematic diagram illustrating the effect of increasing MNPs concentration and PIMA-g-$C_{12}$ amount to the MNPs encapsulation.

Overall, the effect of increasing MNPs concentration and PIMA-g-$C_{12}$ can be summarized in the illustration presented in **Fig. S8**. As the initial MNPs concentration increased or PIMA-g-$C_{12}$ amount increased, there is more PIMA-g-C12 in the proximity of MNPs which lead to decrease in the interdistance between the MNPs and the polymers. Therefore the probability of the MNPs being encapsulated singly by the amphiphilic brush co-polymers increases.

## S7. FT-IR Spectra Analysis of IONPs and WIONPs

In order to obtain powder samples of WIONPs for FT-IR, WIONPs dispersed in water was freeze-dried for 4 days. On the other hand, oleic-acid coated IONPs were washed/precipitated using mixture of acetone/hexane and isolated by using centrifugation. The precipitate was then oven-dried (50$^{o}$C) for few minutes in order to obtain IONPs powder sample. The comparison of the FT-IR spectra of IONPs, PIMA-g-$C_{12}$ and WIONPs were presented in **Figure S9** below.

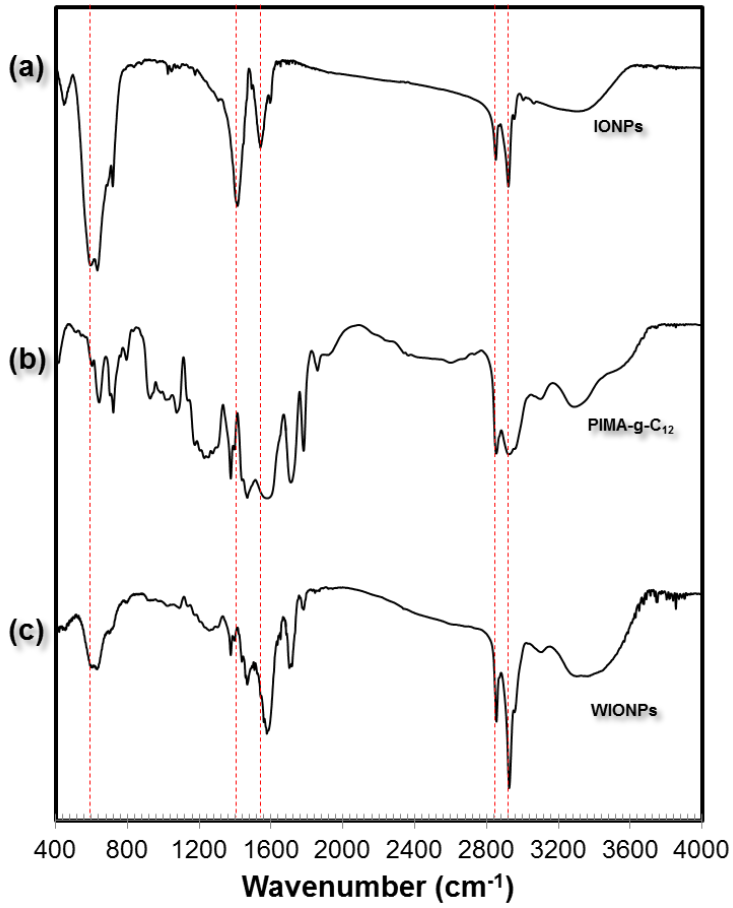


**Fig. S9** FT-IR spectra of (a) oleic acid coated IONPs, (b) PIMA-g-$C_{12}$ and (c) PIMA-g-$C_{12}$ coated IONPs (WIONPs).

It can be observed from the FT-IR spectra that **(1)** For IONPs, the presence of Fe-O stretching at 570-590 $cm^{-1}$ indicated the bonding of oleic acid to the IONPs nanocrystals. The bonding of oleic acid to IONPs involved the formation of $–COO^{–}$ functional group as indicated from the asymmetric and symmetric stretching vibrations of $–COO^{–}$ functional group in the range of 1530-1580 $cm^{-1}$. The presence

of oleic acid were further confirmed by the existence of both asymmetric and symmetric $–CH_2–$ functional group stretching vibrations at around 2916 $cm^{-1}$ and 2848 $cm^{-1}$ as well as the existence of $–CH_3$ functional group bending vibration at 1404 $cm^{-1}$. **(2)** For PIMA-g-$C_{12}$, few characteristic peaks can be observed such as the presence of the absorption peaks at 1605 $cm^{-1}$, 1713 $cm^{-1}$ and 3000-3600 $cm^{-1}$ which corresponded to the C=O stretching bond of amides and carboxylic acids as well as the presence of O–H stretching resonance of the carboxylic acids . The remaining adsorption from C–H bonds (due to alkyl chain $C_{12}$ at 2855 $cm^{-1}$ and 2930 $cm^{-1}$ were also observed). **(3)** After the formation of PIMA-g-$C_{12}$ encapsulated IONPs, few characteristic peaks of both IONPs and PIMA-g-$C_{12}$ were still observed and superimposed to give the WIONPs FTIR spectra, indicating no significant chemical interaction between amphiphilic brush co-polymers and IONPs.

Based on the FT-IR results presented in **Fig. S9**, the coating of IONPs with amphiphilic polymer PIMA-g-$C_{12}$ can only be due to the hydrophobic-hydrophobic interactions between the alkyl chain of oleic acid ($C_{18}$) from IONPs and dodecylamine ($C_{12}$) from PIMA-g-$C_{12}$. The presence of such hydrophobic-hydrophobic interaction between $C_{12}$ and $C_{18}$ helped to keep MNPs remained intact inside the amphiphilic polymer coating.

## S8. Further Characterization of MFNPs

The as-synthesized hydrophobic MFNPs from the thermolysis of metal-acetylacetonate precursors were found to have an average size of 18.9 ± 2.4 nm. Such MFNPs TEM size distribution was obtained by analyzing 150-200 MFNPs nanocrystals from low magnification TEM images (not included) and the size distribution plot was given in **Fig. S10a**. The crystal structure of MFNPs was analyzed by x-ray diffraction experiment. The XRD pattern of MFNPs in **Fig. S10b** was indexed against jacobsite ($MnFe_2O_4$) phase (JCPDS 74-2403). The magnetic property of MFNPs was measured by VSM experiment at 300K and the resultant hysteresis loop profile was given in **Fig. S10c**. Similar to IONPs in section **S2**, MFNPs also exhibited superparamagnetism with negligible coercivity and remnant magnetization ($M_R$). The saturation magnetization ($M_S$) for MFNPs was found to be 97.06 emu.g$^{-1}$.

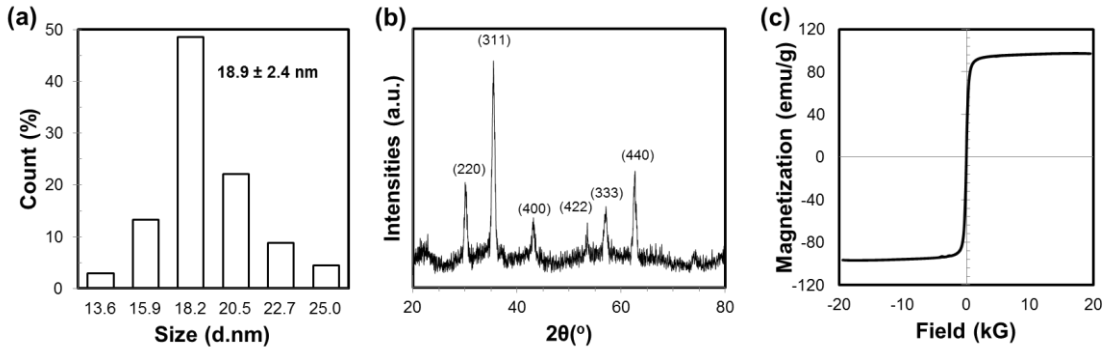


**Fig. S10** (a) TEM size distribution of hydrophobic MFNPs in chloroform. (b) XRD pattern of MFNPs. (c) Hysteresis loop profile of MFNPs recorded at 300K from VSM experiment.

## S9. VSM and TGA Analysis of WMFNPs Sample

A further investigation using VSM showed that after PIMA-g-$C_{12}$ coating, WMFNPs still exhibited superparamagnetism (**Fig. S11a**). The hysteresis loop of WMFNPs samples recorded at 300K indicated that the saturation magnetization ($M_S$ value) of WMFNPs was 14.78 emu.g$^{-1}$. The overall decrease in MFNPs $M_S$ value from 97.06 emu.g$^{-1}$ (approximately 84.77%) was due to the presence of PIMA-g-$C_{12}$ coating. The presence of PIMA-g-$C_{12}$ was further confirmed by the thermal-gravimetric analysis (TGA) results of WMFNPs. As indicated in **Fig. S11b**, it was found out that the remaining 16.08% weight of WMFNPs after heating to 750$^{o}$C at 10$^{o}$C/Min was due to the presence of inorganic components (MFNPs). Approximately, around 83.92% WMFNPs weight loss was due to the presence of organic components (*i.e.* PIMA-g-$C_{12}$). The increase in the organic components amount (as compared to the inorganic components) due to PIMA-g-$C_{12}$ coating contributed to the decrease in the overall mass saturation magnetization value.

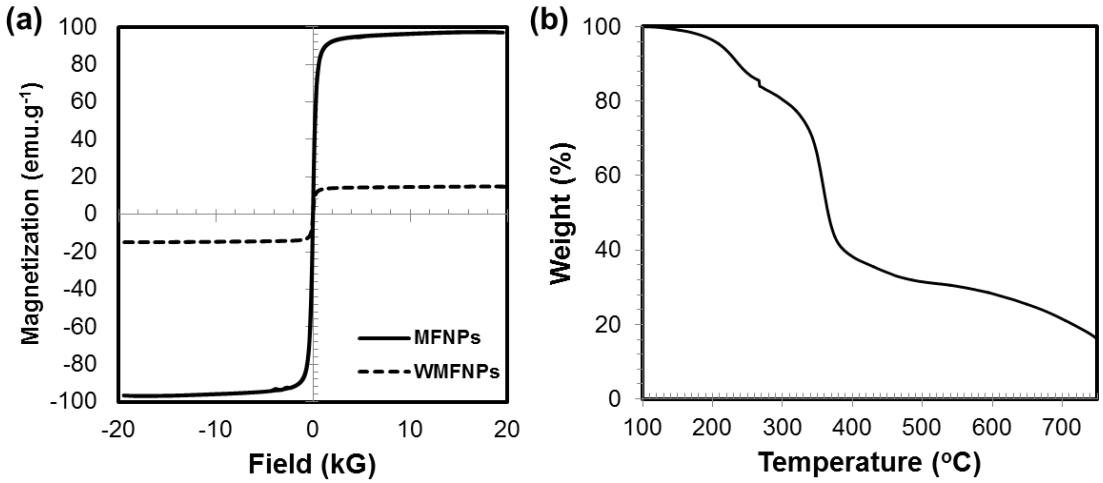


**Fig. S11** (a) Comparison of magnetic hysteresis loop profile of MFNPs (solid line) and WMFNPs (dotted line). (b) TGA heating profile of WMFNPs under $N_2$ atmosphere.

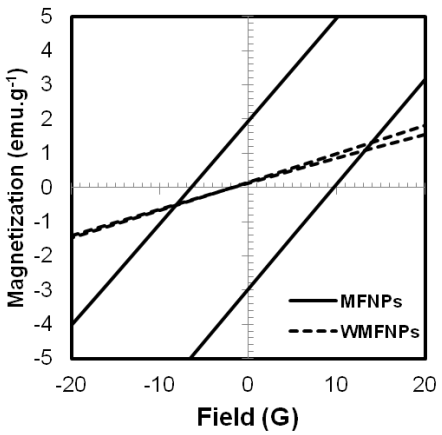


**Fig. S12** Magnified magnetic hysteresis loops of MFNPs (solid line) and WMFNPs (dotted line).

The magnified magnetic hysteresis loop of MFNPs given in **Fig. S12**, showed 2-3 emu.g$^{-1}$ remnant magnetization ($M_R$) which indicated slight magnetic coupling between the hydrophobic oleic-aid coated MFNPs. However, after coating with PIMA-g-$C_{12}$, it can be observed that such remnant magnetization disappeared, signifying that the presence of the low molecular weight amphiphilic brush co-polymer PIMA-g-$C_{12}$ was able to encapsulate/isolate each individual nanoparticle. The complete absence of the remnant magnetization also showed that the steric hindrance between the amphiphilic brush co-polymers coatings would distance the MNPs to each other, minimizing the dipole-dipole interaction. The absence of this magnetic coupling clearly explained the excellent colloidal stability of WMFNPs samples.

**S10. Other Type of Polymer: Poly (Maleic Anhydride-*alt*-1-Octadecene)**

In order to further verify the optimized parameters described in section **S6** of this supporting information, we employed another commercially available amphiphilic brush co-polymers poly (maleic anhydride-*alt*-1-octadecene) or denoted as **PMAO**. By retaining the previously mentioned optimized parameters (initial MNPs concentration = 50mg.mL$^{-1}$; $NP_{ratio}$ = 10, NaOH/carboxyl molar ratio = 2), MFNPs were successfully water solubilized using PMAO. The TEM image of PMAO coated MFNPs can be found in **Fig. S13a**. The inset in **Fig. S13a** showed the high resolution TEM image of PMAO coated MFNPs. As reflected in **Fig. S13b**, the hydrodynamic size of the PMAO coated MFNPs in NaOH and in PBS 1x were recorded to be 30.8 ± 0.2 nm and 32.5 ± 0.2 nm respectively from the DLS experiment (at 25$^{o}$C). No significant aggregation was observed either from the low magnification TEM image or the DLS results.

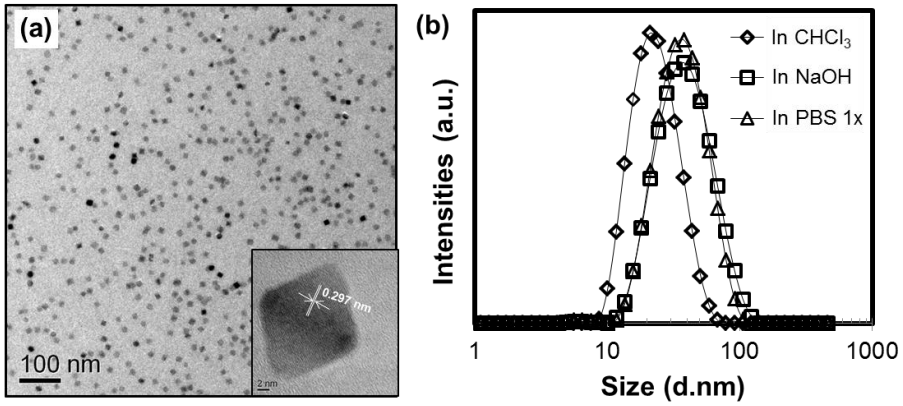


**Fig. S13.** (a) TEM image of MFNPs encapsulated with poly (maleic anhydride-*alt*-1-octadecene) or PMAO (inset: high resolution TEM image of MFNPs; *d*-spacing of 0.297 nm corresponded to (220) plane of MFNPs). (b) Size distribution of MFNPs encapsulated with PMAO in various solvents, e.g. $CHCl_3$, NaOH and PBS 1x (from DLS experiment).

The experimental procedures to obtained PMAO coated MFNPs were more or less similar to the PIMA-g-$C_{12}$ coated MFNPs with slight modification as described briefly below:

*1. Materials:* Poly (maleic anhydride-*alt*-1-octadecene) (or **PMAO**; m.w. 30000-50000) was obtained from Sigma-Aldrich. Chloroform ($CHCl_3$; 99.99%) was obtained from Fisher Scientific. Sodium hydroxide (pellets; 97.0%) were used as received.

*2. MFNPs Water Solubilization Using PMAO:* Briefly 1 mL of MFNPs (in $CHCl_3$ ;50 $mg.mL^{-1}$) was mixed with 10 mL of PMAO (in $CHCl_3$; 100 $mg.mL^{-1}$). The $\mathbf{NP}_{ratio}$ was maintained at 10. The mixture of MFNPs/PMAO was then sonificated for 10-20 minutes in an ultrasonic bath. Subsequently the solvent ($CHCl_3$) was then evaporated by nitrogen gas blowing for 1 hour. The thin layer of PMAO/MNPs composite film was then further dried *in vacuo* for 1 day. The resulting dried film was then re-dissolved into 11.25 mL of 1.0 M sodium hydroxide with the aid of ultrasonic bath for 60 minutes at 60$^{o}$C. Sodium hydroxide was removed through dialysis against Millipore® water (dialysis MWCO: 12-14kDa) and excess polymers were removed through the aid of centrifugation.

*3. Materials Characterization:* The TEM image of PMAO coated MFNPs was obtained under TEM (JEOL 3010; 300kV). The hydrodynamic diameter of PMAO coated MFNPs was measured using a Malvern Zetasizer Nano-ZS.

## S11. Water Solubilization – Hydrodynamic Size Summary

**Table S2.** Summary of IONPs and MFNPs (coated with PIMA-g-$C_{12}$ as well as PMAO amphiphilic brush co-polymers) hydrodynamic size.

| Nanocrystals | Coatings | Solvent | Average $d_{hyd}$ (nm) | Size Change w.r.t Hydrophobic MNPs |
|---|---|---|---|---|
| **IONPs ($Fe_3O_4$)** | Oleic Acid | $CHCl_3$ | 15.6 ± 0.1 | - |
| | PIMA-g-$C_{12}$ | NaOH | 18.5 ± 0.1 | 17.97% |
| | PIMA-g-$C_{12}$ | PBS 1x | 19.6 ± 0.3 | 25.06% |
| **MFNPs ($MnFe_2O_4$)** | Oleic Acid | $CHCl_3$ | 22.7 ± 0.1 | - |
| | PIMA-g-$C_{12}$ | NaOH | 26.3 ± 0.1 | 15.88% |
| | PIMA-g-$C_{12}$ | PBS 1x | 30.1 ± 0.1 | 32.56% |
| **MFNPs ($MnFe_2O_4$)** | PMAO ($C_{18}$) | NaOH | 30.8 ± 0.2 | 35.50% |
| | PMAO ($C_{18}$) | PBS 1x | 32.5 ± 0.2 | 42.98% |

Note: (a) Initial MNPs concentration = 50 $mg.mL^{-1}$, (b) NaOH/Carboxyl molar ratio = 2:1 and (c) PIMA-g-$C_{12}$/MNPs mass ratio = 10:1.

In **Table S2** above, the hydrodynamic size of both IONPs and MFNPs in $CHCl_3$ as well as in aqueous phase were described. The percentage of the hydrodynamic size increment from the water solubilizaiton procedures was calculated. The increments in the hydrodynamic size were found to be around 25-43%. Such increments in the hydrodynamic size indicated higher probability that IONPs and MFNPs were indeed single encapsulated during the process.

## Reference:

[1]. R. Di Corato, A. Quarta, P. Piacenza, A. Ragusa, A. Figuerola, R. Buonsanti, R. Cingolani, L. Manna and T. Pellegrino, *Journal of Materials Chemistry*, 2008, **18**, 1991-1996.

[2]. E. E. Lees, T.-L. Nguyen, A. H. A. Clayton and P. Mulvaney, *ACS Nano*, 2009, **3**, 1121-1128.

[3]. T. Pellegrino, L. Manna, S. Kudera, T. Liedl, D. Koktysh, A. L. Rogach, S. Keller, J. Rädler, G. Natile and W. J. Parak, *Nano Letters*, 2004, **4**, 703-707.

[4]. M. Moros, B. Pelaz, P. Lopez-Larrubia, M. L. Garcia-Martin, V. Grazu and J. M. de la Fuente, *Nanoscale*, 2010, **2**, 1746-1755.

[5]. W. W. Yu, E. Chang, J. C. Falkner, J. Zhang, A. M. Al-Somali, C. M. Sayes, J. Johns, R. Drezek and V. L. Colvin, *Journal of the American Chemical Society*, 2007, **129**, 2871-2879.

[6]. L. M. Bronstein, E. V. Shtykova, A. Malyutin, J. C. Dyke, E. Gunn, X. Gao, B. Stein, P. V. Konarev, B. Dragnea and D. I. Svergun, *The Journal of Physical Chemistry C*, 2010, **114**, 21900-21907.

[7]. M. Gonzales and K. M. Krishnan, *Journal of Magnetism and Magnetic Materials*, 2007, 311, 59-62.

[8]. (a). J. Yang, S. R. Dave and X. Gao, *Journal of the American Chemical Society*, **2008**, 130, 5286-5292. (b). D. Janczewski, N. Tomczak, M.-Y. Han and G. J. Vancso, *Nat. Protocols*, 2011, **6**, 1546-1553. (c). U. I. Tromsdorf, N. C. Bigall, M. G. Kaul, O. T. Bruns, M. S. Nikolic, B. Mollwitz, R. A. Sperling, R. Reimer, H. Hohenberg, W. J. Parak, S. Förster, U. Beisiegel, G. Adam and H. Weller, *Nano Letters*, 2007, **7**, 2422-2427. (d). L. Yuwen, B. Bao, G. Liu, J. Tian, H. Lu, Z. Luo, X. Zhu, F. Boey, H. Zhang and L. Wang, *Small*, 2011, n/a-n/a. (e). E. V. Shtykova, A. Malyutin, J. Dyke, B. Stein, P. V. Konarev, B. Dragnea, D. I. Svergun and L. M. Bronstein, *The Journal of Physical Chemistry C*, 2010, **114**, 21908-21913. (f). E. V. Shtykova, X. Huang, X. Gao, J. C. Dyke, A. L. Schmucker, B. Dragnea, N. Remmes, D. V. Baxter, B. Stein, P. V. Konarev, D. I. Svergun and L. M. Bronstein, *The Journal of Physical Chemistry C*, 2008, **112**, 16809-16817. (g). D. Janczewski, N. Tomczak, Y. W. Khin, M.-Y. Han and G. Julius Vancso, *European Polymer Journal*, 2009, **45**, 3-9. (h). C.-A. J. Lin, R. A. Sperling, J. K. Li, T.-Y. Yang, P.-Y. Li, M. Zanella, W. H. Chang and W. J. Parak, *Small*, 2008, **4**, 334-341. (i). W. Y. William and et al., *Nanotechnology*, 2006, **17**, 4483.

[9]. E. S. Guang Choo, X. Tang, Y. Sheng, B. Shuter and J. Xue, *Journal of Materials Chemistry*, 2011, **21**, 2310-2319.